Improving smartphone-based positioning accuracy with height constraint and application to pedestrian and vehicular positioning

Farzaneh Zangenehnejad$^{\boxtimes}$ and Yang Gao

Department of Geomatics Engineering, Schulich School of Engineering, University of Calgary,
Calgary, AB T2N 1N4, Canada

Emails: zangenehnej@ucalgary.ca; ygao@ucalgary.ca

$\boxtimes$ Corresponding author

Abstract: Since the release of Android version 7 in 2016, the smartphone users have had access to the raw global navigation satellite system (GNSS) measurements (i.e., pseudorange, carrier-phase, Doppler, and carrier-to-noise density ratio (C/N0)) through the new application programming interface (API) called android location (API level 24). This capability opens opportunities to apply different positioning techniques, ranging from absolute to differential techniques, to the smartphone observations. Precise point positioning (PPP) is a powerful method for conducting accurate real-time positioning using a single receiver, and it can be applied to the smartphone observations as well. Most PPP smartphone positioning studies have so far focused on utilizing the GNSS only observations obtained from the smartphone's API. However, incorporating additional information as constraints, such as height information, can enhance accuracy and overall stability. Although the vertical positioning accuracy of GNSS is generally lower than the horizontal accuracy, utilizing recorded height from the smartphone GNSS chipset can still be beneficial. This incorporation increases the degree of freedom and strengthens the geometry between the receiver and satellites. In this study, we assess the effectiveness of the uncombined PPP (UPPP) model in the presence of height constraints. We utilize both pedestrian walking and vehicular datasets collected by a dual-frequency Xiaomi Mi8 device to evaluate the effect of adding height constraint to PPP model. The results demonstrate an average improvement of 22% and 26% on the root-mean-square (RMS) of horizontal error and the 50th percentile error, respectively, when employing the height constraints UPPP model. Additionally, the findings indicated a decrease in PPP convergence time, further supporting the positive impact of incorporating height constraints.

Dr. Zhizhao Liu

1. Introduction

The growing need for highly accurate location information in mass-market applications has driven the development of numerous smartphone-based location-based services (LBS) utilizing the GNSS technology. In 2016, Google announced the availability of raw GNSS observations, including pseudorange, carrier-phase, Doppler shift, and carrier-to-noise density ratio (C/N0) observations, to the users and developers. This has opened significant opportunities for the development of LBS based on smartphones. The increasing number of smartphone models capable of providing raw GNSS observations has led to a demand for improving the positioning accuracy with smartphones. Different positioning algorithms, such as single point positioning (SPP), precise point positioning (PPP), real-time kinematic (RTK) method and GNSS/INS integration positioning method, have been investigated for accuracy improvement of smartphone-based positioning. The reader can find a thorough overview of recent advancements and research in GNSS smartphone positioning carried out until 2021 in Paziewski (2020) and Zangenehnejad and Gao (2021). Since this contribution focused on the use of PPP, we will highlight some important and relevant contributions in this field.

Several researchers have proposed modified PPP models, including improved stochastic modelling, modifications to the PPP model, multi-constellation multi-frequency PPP and PPP-RTK, to enhance smartphone positioning performance. Guo et al. (2020) investigated the GNSS observations of a Xiaomi Mi8 device, identifying a significant

correlation between the pseudorange noise and C/N0 records, which have been previously noted by several researchers. They then introduced a C/N0-dependent weighting model for GNSS positioning and implemented a time-differenced (TD) positioning filter to take advantage of high-precision carrier-phase observations, achieving satisfying results specially with the inclusion of L5/E5 observations. Li et al. (2022a) introduced a combined elevation angle and C/N0 weighting method for the smartphone-based GNSS PPP, resulting in a 22.7% and 24.2% improvement in 3D positioning accuracy in open-sky areas, and a 52.0% and 26.0% improvement in areas with limited visibility compared to the elevation-angle-only and C/N0-only weighting models, respectively. Zangenehnejad and Gao (2023) used the least-square variance component estimation (LS-VCE) method to stochastic modeling of noisy smartphone GNSS observations, finding no significant correlation between pseudorange and carrier-phase observations of GPS and GLONASS on the L1 frequency. They demonstrated that the quality of GLONASS carrier-phase observations is comparable to that of GPS. They then showed a significant improvement of 25.1% and 32.7% in horizontal positioning RMS and the 50th percentile error employing the obtained stochastic model.

Chen et al. (2019) introduced a modified single-frequency PPP algorithm to manage evolving differences (inconsistency) between the pseudorange and carrier-phase observations by estimating distinct clock biases for each. The modified real-time PPP algorithm resulted in average horizontal and vertical RMS errors of 0.81 meters and 1.65 meters, respectively. Li et al. (2023) also proposed a customized UPPP model which addresses the inconsistency between code and carrier-phase observations using the Huawei P40 device. Their findings demonstrated enhanced positioning accuracy, achieving below 0.2 m in static scenarios and approximately 1.0 m in kinematic scenarios, which represents an improvement compared to UPPP without addressing code-carrier inconsistency. Elmezayen and El-Rabbany (2019) achieved decimeter-level positioning accuracy in both post-processing and real-time static PPP modes and meter-level accuracy in kinematic mode using a Xiaomi Mi8 with combined GPS/Galileo dual-frequency observations. Wu et al. (2019) utilized the dual-frequency GPS (L1/L5) and Galileo (E1/E5a) observations of a Xiaomi Mi8 device. They achieved centimeter-level accuracy in static mode but meter-level accuracy in kinematic mode using the PPP algorithm with the ionosphere-free combination. Li and Cai (2022) proposed a mixed single- and dual-frequency quad-constellation PPP model to enhance the smartphone positioning accuracy, showing improved performance compared to the traditional dual-frequency and single-frequency PPP models in both static and kinematic tests. Recently, there has also been notable interest in PPP-RTK for enhancing the positioning accuracy and reducing the PPP convergence time (Li et al. 2022b).

Despite considerable efforts in this field, achieving high accuracy smartphone-based positioning still remains a significant challenge, typically limited to (sub)meter-level accuracy. Most of these studies have focused on the usage of smartphone GNSS observations only, coming from the location smartphone's API. However, the incorporation of supplementary information as constraints has the potential to improve both accuracy and overall stability. Such supplementary information can originate from either internal sensors such as the inertial measurement unit (IMU) sensor or external sources such as camera observations, digital map data, and WiFi signals, etc. An additional type of information that can be utilized is the IMU sensor data. They can be integrated with the smartphone GNSS observables to achieve a better localization solution. Zhu et al. (2022) proposed an IMU-aided uncombined PPP coupled mathematical model, suitable for smartphone positioning. The proposed PPP/INS-coupled model integrated the dual-frequency GNSS observations and IMU data from smartphones with C/N0-dependent stochastic model and robust Kalman filter (RKF) model to improve the positioning performance under GNSS-degraded environments. Experimental results indicated that the proposed PPP/INS method could effectively improve the smartphone positioning performance compared with the conventional smartphone PPP method. Yi et al. (2022) presented a novel sensor fusion technique using PPP and the inertial sensors in smartphones, combined with a single- and dual-frequency (SFDF) optimization scheme for smartphones. A significant improvement in the final solutions has been confirmed in the case of multi-GNSS PPP/IMU integration, providing consistent horizontal positioning accuracy of <2 m RMS in real-world driving scenarios.

Another type of information that can be utilized for accuracy improvement is the height information to be integrated as the weighted constraints. Several research studies have investigated the accuracy of indoor smartphone-based positioning by considering the impact of incorporating height information estimated from the smartphone's built-in barometer (Shin et al. 2016, Albéri et al. 2017, Landa et al. 2018 and Zhao et al. 2019). These studies utilized the smartphone's built-in barometer to calculate the pedestrian height using the atmospheric pressure. For example, Kim et al. (2012) used a barometer to estimate height location of pedestrians and designed a KF to minimize the height error. Abdulrahim et al. (2012) proposed a height limitation method based on

height change of adjacent steps to correct the height error. In indoor environments, the accuracy of the barometer heights may outperform that of the GNSS heights. In this contribution, however, we focus on the application of the GNSS technique for outdoor positioning. Therefore, we will utilize the GNSS chipset heights estimates to improve the accuracy of both pedestrian and vehicular positioning with smartphones. The Android system has a set of functions called API, allowing users to use the system's features. Each version of Android has different types of APIs. The android.location API includes classes for location-related services, and one of them is the "Location" class, which provides access to the GNSS chipset solution. However, the functionality of the position chipset calculation is a black box for users as it is not publicly disclosed. Nevertheless, it is evident that the chipset position determination does not solely rely on the GNSS observations. For instance, when entering areas where there were no GNSS signals such as underpasses or underground parking lots, the device continues to provide position output. This indicates the chipset has utilized other sensors in a sensor fusion approach, integrating likely available Inertial Navigation Systems (INS), WiFi signals, and other sensors in addition to the GNSS observations. The "Location" class consists of latitude and longitude in the WGS84 coordinate system, altitude, timestamp, accuracy, and other information such as bearing and velocity. The reader can find more information about the "Location" class at https://developer.android.com/reference/android/locat ion/Location. The "AltitudeMeters" from this class provides the height above the WGS84 ellipsoid in meters. It is accessible for different providers such as GPS, fused, network, etc. In this research, we specifically use the recorded "AltitudeMeters" values for the GPS provider.

This paper is structured as follows. First, a brief review of the UPPP model is provided. How to incorporate the height constraints into the estimation procedure is also outlines in this section. Following that, we assess the performance of adding height constraints to the UPPP model using several GNSS observations from the Xiaomi Mi8 device in both pedestrian walking and vehicular experiments. Finally, some conclusions are made in the last section.

2. Precis point positioning (PPP)

The PPP method is a single-receiver GNSS-based precise positioning technique. It is different from the RTK technique, which typically requires a base station (Zumberge 1997; Kouba and Héroux 2001 and Héroux et al. 2014). Currently there is a high demand on improving the PPP accuracy with smartphones especially in kinematic mode. In this contribution, we aim to investigate how introducing height constraints affects the performance of PPP using Android smartphones. This section consists of two subsections, the first section provides some explanations about the functional model (uncombined PPP) used in the contribution while in the second section, how to introduce the height constraints into the mathematical model will be described.

2.1 Functional model

In this study, we utilize the uncombined PPP model as the functional model, indicating that we use the undifferenced observations of each frequency without making any combination between them. The undifferenced GNSS code and carrier-phase observations for the satellite s and the receiver r on frequency j are as follows (Teunissen, and Kleusberg 1998)

$$E\left(\mathrm{P}_{r,j}^s\right) = \rho_r^s + T_r^s + cdt_r - cdt^s + \gamma_j I_{r,1}^s + b_{r,j} + b_j^s$$

$$E\left(\Phi_{r,j}^s\right) = \rho_r^s + T_r^s + cdt_r - cdt^s - \gamma_j I_{r,1}^s + \lambda_j N_{r,j}^s + B_{r,j} + B_j^s$$

(1)

where P_j and Φ_j represent the pseudorange and carrier-phase observations on frequency j in meters, $\rho = \sqrt{(X^s - X_r)^2 + (Y^s - Y_r)^2 + (Z^s - Z_r)^2}$ is the geometric range between satellite and receiver which is a function of the satellite coordinate (X^s, Y^s, Z^s) and the receiver coordinate (X_r, Y_r, Z_r), T denotes the tropospheric delay (m) which can be separated into dry and wet parts, c is the vacuum speed of light (m/s), dt_r and dt^s are the receiver and satellite clock errors (s), respectively, $I_{r,1}^s$ is the first-order slant ionospheric delay on the first frequency L1 (m), $\gamma_j = f_1^2/f_j^2$ is the frequency-dependent multiplier factor (in the case of L1 frequency $\gamma_j = 1$), f_j is the

corresponding frequency, λ_j is the corresponding carrier-phase wavelength (m), $N_{r,j}^s$ denotes the integer carrier-phase ambiguity term in cycle, $b_{r,j}$ and $B_{r,j}$ denote the frequency-dependent receiver pseudorange and carrier-phase hardware delays (biases), respectively, and b_j^s and B_j^s are the frequency-dependent satellite pseudorange and carrier-phase hardware delays (biases), respectively.

The International GNSS Service (IGS) provides satellite clock error data derived from the ionosphere-free linear combination of code observations on the L1 and L2 frequencies (i.e., P1 and P2) (Kouba and Héroux 2001). However, incorporating these satellite

clock errors into the PPP model for the original code and carrier-phase observations introduces an additional observation bias, requiring the consideration of satellite differential code biases (DCB). The DCBs are also available from the IGS.

Assuming the precise satellite clock errors $cdt^{s,IF}$ provided by the IGS as $cdt^{s,IF} = cdt^s - b_{IF(1,2)}^s$ where $b_{IF(1,2)}^s = \alpha_{IF}^{1,2} b_1^s + \beta_{IF}^{1,2} b_2^s$ is the satellite

ionosphere-free code bias, with the coefficients as follows:

$$\left.\begin{array}{l} \alpha_{IF}^{i,j} = f_i^2 / (f_i^2 - f_j^2) \\ \beta_{IF}^{i,j} = 1 - \alpha_{IF}^{i,j} = -f_j^2 / (f_i^2 - f_j^2) \end{array}\right\} \qquad (2)$$

with availability of the precise satellite clock errors $cdt^{s,IF}$, one can rewrite the uncombined PPP model for the L1 and L5 frequencies as follows:

$$E(P_{r,1}^s) = \rho_r^s + T_r^s + (cdt_r + b_{r,1}) - cdt^{s,IF} + I_{r,1}^s + b_1^s - b_{IF(1,2)}^s$$

$$E(\Phi_{r,1}^s) = \rho_r^s + T_r^s + (cdt_r + b_{r,1}) - cdt^{s,IF} - I_{r,1}^s + \lambda_1 N_{r,1}^s + B_{r,1} + B_1^s - b_{IF(1,2)}^s - b_{r,1}$$

$$E(P_{r,3}^s) = \rho_r^s + T_r^s + (cdt_r + b_{r,1}) - cdt^{s,IF} + \gamma_3 I_{r,1}^s + b_{r,3} - b_{r,1} + b_3^s - b_{IF(1,2)}^s$$

$$E(\Phi_{r,3}^s) = \rho_r^s + T_r^s + (cdt_r + b_{r,1}) - cdt^{s,IF} - \gamma_3 I_{r,1}^s + \lambda_3 N_{r,3}^s + B_{r,3} + B_3^s - b_{IF(1,2)}^s - b_{r,1}$$

(3)

In this equation, $b_1^s - b_{IF(1,2)}^s = -\frac{1}{\gamma_2 - 1} DCB_{1,2}^s$ and $b_3^s - b_{IF(1,2)}^s = DCB_{1,3}^s + \frac{1}{\gamma_2 - 1} DCB_{1,2}^s$ are functions of inter frequency satellite DCBs where $DCB_{ij}^s = b_i^s - b_j^s$ is the satellite DCBs between the ith and jth frequency bands (Schaer al. 1998; Dach et al. 2015). Multi-GNSS inter frequency satellite DCBs are currently provided by some IGS MGEX centers, such

as the Institute of Geodesy and Geophysics (IGG) of the Chinese Academy of Sciences (CAS) (Wang et al. 2016) and the German Aerospace Center (Montenbruck et al. 2014). When external inter frequency satellite DCBs are available, the observation minus calculation (OMC) terms of Eq. (3) can be rewritten as follows:

$$\begin{cases} E\left(\delta P_{r,1}^s + cdt^{s,IF} + \frac{1}{\gamma_2 - 1} DCB_{1,2}^s\right) = G\Delta x_r + T_r^s + \overline{cdt_r} + I_{r,1}^s \\ E\left(\delta\Phi_{r,1}^s + cdt^{s,IF}\right) = G\Delta x_r + T_r^s + \overline{cdt_r} - I_{r,1}^s + \lambda_1 \bar{N}_{r,1}^s \\ E\left(\delta P_{r,3}^s + cdt^{s,IF} + DCB_{1,3}^s + \frac{1}{\gamma_2 - 1} DCB_{1,2}^s\right) = G\Delta x_r + T_r^s + \overline{cdt_r} + \gamma_3 I_{r,1}^s - DCB_{1,3}^r \\ E\left(\delta\Phi_{r,3}^s + cdt^{s,IF}\right) = G\Delta x_r + T_r^s + \overline{cdt_r} - \gamma_3 I_{r,1}^s + \lambda_3 \bar{N}_{r,3}^s \end{cases}$$

(4)

where δ is the OMC notation, G is a vector containing the line-of-sight components between satellite and receiver ($G = \begin{bmatrix} \frac{\partial \rho}{\partial X_r} & \frac{\partial \rho}{\partial Y_r} & \frac{\partial \rho}{\partial Z_r} \end{bmatrix}$), Δx_r is the receiver position increment error, $\overline{cdt_r} = cdt_r + b_{r,1}$, $DCB_{1,3}^r = b_{r,1} - b_{r,3}$, $\lambda_1 \bar{N}_{r,1}^s = \lambda_1 N_{r,1}^s + B_{r,1} + B_1^s - b_{IF(1,2)}^s - b_{r,1}$ and $\lambda_3 \bar{N}_{r,3}^s = \lambda_3 N_{r,3}^s + B_{r,3} + B_3^s - b_{IF(1,2)}^s - b_{r,1}$. The unknowns here are the receiver position, the receiver clock error $\overline{cdt_r}$, the real-valued carrier-phase ambiguity terms $\lambda_1 \bar{N}_{r,1}^s$ and $\lambda_3 \bar{N}_{r,3}^s$, the zenith wet delay and the receiver differential code bias between L1 and L5 frequency $DCB_{1,3}^r$. The slant ionospheric delay on the L1 frequency $I_{r,1}^s$ can be either estimated or modeled.

2.2 Height constraint UPPP model

Let us assume the general equation of the World Geodetic System (WGS)-84 reference ellipsoid as follows

$$\frac{X^2 + Y^2}{a^2} + \frac{Z^2}{b^2} = 1 \qquad (5)$$

where a and b are the semi-major and semi-minor axes of the WGS-84 reference ellipsoid, respectively. Incorporating the height information (h) as weighted constraints ($h = c$ with σ_h) in the observation equations requires converting the height to the Earth-centered, Earth-fixed (ECEF) frame (X, Y, Z) since the unknowns are in that frame. Let's suppose that the height constraint can be stated as follows:

$$h = f(X_r, Y_r, Z_r) \qquad (6)$$

where h is a function of the receiver ECEF coordinates (i.e., X_r, Y_r, Z_r). The specific details and expression of the function f can be found in Hofmann-Wellenhof's work (2012). The height constraint can be approximately expressed as follows (Phatak et al. 1999 and Liu et al. 2020):

$$\frac{X_r^2 + Y_r^2}{(a+h)^2} + \frac{Z_r^2}{(b+h)^2} = 1 \qquad (7)$$

which is a highly reliable approximation given that h is much smaller than a and b. Next, we need to take

69

partial derivatives of h with respect to the receiver ECEF coordinates (i.e., X_r, Y_r, Z_r). These derivatives are of the form (Phatak et al. 1999 and Liu et al. 2020):

$$\begin{cases} \frac{\partial h}{\partial X_r} = \frac{X_r(a+h)(b+h)^3}{(b+h)^3(X_r^2+Y_r^2)+(a+h)^3 Z_r^2} \\ \frac{\partial h}{\partial Y_r} = \frac{Y_r(a+h)(b+h)^3}{(b+h)^3(X_r^2+Y_r^2)+(a+h)^3 Z_r^2} \\ \frac{\partial h}{\partial Z_r} = \frac{Z_r(a+h)^3(b+h)}{(b+h)^3(X_r^2+Y_r^2)+(a+h)^3 Z_r^2} \end{cases} \quad (8)$$

and

$$\delta h = \frac{\partial h}{\partial X_r}dX_r + \frac{\partial h}{\partial Y_r}dY_r + \frac{\partial h}{\partial Z_r}dZ_r \quad (9)$$

Eq. (9) will be used as the height constraint added to the observation equation.

Now let's assume that the linearized form of observation equations of each UPPP form is expressed as $\delta y = A\delta x + \varepsilon$ where $\delta y = [\delta P_{L_1} \quad \delta P_{L_5} \quad \delta \Phi_{L_1} \quad \delta \Phi_{L_5} \quad \delta h]^T$ is the observation vector including pseudorange and carrier-phase observations as well as the height information added to the observation equations as the weighted constraints, ε denotes the unmodeled errors of the observations, and $A = [A_P^T \quad A_\Phi^T \quad A_h^T]^T$ is the design matrix defined as follows:

$$A_P = \begin{bmatrix} G & e & 0 & mpf & I & 0 & 0 \\ G & e & -e & mpf & \gamma_3 I & 0 & 0 \end{bmatrix}$$
$$A_\Phi = \begin{bmatrix} G & e & 0 & mpf & -I & I & 0 \\ G & e & 0 & mpf & -\gamma_3 I & 0 & I \end{bmatrix} \quad (10)$$
$$A_h = \begin{bmatrix} \frac{\partial h}{\partial X_r} & \frac{\partial h}{\partial Y_r} & \frac{\partial h}{\partial Z_r} & 0 & 0 & 0 & 0 & 0 \end{bmatrix}$$

with the unknowns Δx_r, $\overline{cdt}_r$, $DCB_{1,3}^r$, ZWD, $I_{r,1}^s$, $\lambda_1 \overline{N}_{r,1}^s$ and $\lambda_3 \overline{N}_{r,3}^s$ (the receiver position, the receiver clock error, the real-valued carrier-phase ambiguity terms, the zenith wet delay and the receiver differential code bias between L1 and L5 frequency). The slant ionospheric delay on the L1 frequency $I_{r,1}^s$ can be modeled. In this contribution, the GIM is used as the external ionosphere information to model the ionospheric error. Therefore, the columns related to the slant ionospheric delays should be removed. In Eq. (10), G is a vector consisting of the partial derivatives of the geometric distance between the satellite and the receiver with respect to the receiver coordinates, e is an array of all ones, mpf is a vector containing the tropospheric mapping functions and I is the identity matrix.

Finally, we need to decide where to obtain height information. The android.location API, part of Android, includes the "Location" class containing details such as latitude, longitude, altitude (provided in the WGS84 coordinate system), and so on. More details can be found at developer.android.com/reference/android/location/Lo

cation. In this research, we use the "AltitudeMeters" values for the GPS provider with a standard deviation of $\sigma_h = 10$ cm. These values are recorded by the GnssLogger App and saved into a CSV file.

2.3 Simulation example

To demonstrate the effectiveness of integrating height constraints into the positioning performance, simulations are conducted for a basic GNSS positioning case of four satellites. The design matrix for four satellites takes the form (Hofmann-Wellenhof 2012):

$$A = \begin{bmatrix} -\frac{X^1-X_r}{\rho^1} & -\frac{Y^1-Y_r}{\rho^1} & -\frac{Z^1-Z_r}{\rho^1} & 1 \\ -\frac{X^2-X_r}{\rho^2} & -\frac{Y^2-Y_r}{\rho^2} & -\frac{Z^2-Z_r}{\rho^2} & 1 \\ -\frac{X^3-X_r}{\rho^3} & -\frac{Y^3-Y_r}{\rho^3} & -\frac{Z^3-Z_r}{\rho^3} & 1 \\ -\frac{X^4-X_r}{\rho^4} & -\frac{Y^4-Y_r}{\rho^4} & -\frac{Z^4-Z_r}{\rho^4} & 1 \end{bmatrix} \quad (11)$$

In a local apparent (LA) system, the design matrix A simplifies to

$$A = \begin{bmatrix} -\cos E_1 \cos\alpha_1 & -\cos E_1 \sin\alpha_1 & -\sin E_1 & 1 \\ -\cos E_2 \cos\alpha_2 & -\cos E_2 \sin\alpha_2 & -\sin E_2 & 1 \\ -\cos E_3 \cos\alpha_3 & -\cos E_3 \sin\alpha_3 & -\sin E_3 & 1 \\ -\cos E_4 \cos\alpha_4 & -\cos E_4 \sin\alpha_4 & -\sin E_4 & 1 \end{bmatrix} \quad (12)$$

where E_i and α_i are the elevation angle and azimuth of the satellites, respectively. Adding the height constraint to the above problem can be done as follows:

$$A_{const} =$$
$$\begin{bmatrix} -\cos E_1 \cos\alpha_1 & -\cos E_1 \sin\alpha_1 & -\sin E_1 & 1 \\ -\cos E_2 \cos\alpha_2 & -\cos E_2 \sin\alpha_2 & -\sin E_2 & 1 \\ -\cos E_3 \cos\alpha_3 & -\cos E_3 \sin\alpha_3 & -\sin E_3 & 1 \\ -\cos E_4 \cos\alpha_4 & -\cos E_4 \sin\alpha_4 & -\sin E_4 & 1 \\ \frac{\partial h}{\partial X_r} & \frac{\partial h}{\partial Y_r} & \frac{\partial h}{\partial Z_r} & 0 \end{bmatrix} \quad (13)$$

where $\frac{\partial h}{\partial X_r}$, $\frac{\partial h}{\partial Y_r}$ and $\frac{\partial h}{\partial Z_r}$ are to be replaced with the values obtained from Eq (8). The covariance matrix of the estimates in ECEF frame can be expressed as:

$$Q_{\hat{x}} = (A^T A)^{-1} =$$
$$\begin{bmatrix} \sigma_{X_r}^2 & \sigma_{X_r Y_r} & \sigma_{X_r Z_r} & \sigma_{X_r cdt} \\ \sigma_{X_r Y_r} & \sigma_{Y_r}^2 & \sigma_{Y_r Z_r} & \sigma_{Y_r cdt} \\ \sigma_{X_r Z_r} & \sigma_{Y_r Z_r} & \sigma_{Z_r}^2 & \sigma_{Z_r cdt} \\ \sigma_{X_r cdt} & \sigma_{Y_r cdt} & \sigma_{Z_r cdt} & \sigma_{cdt}^2 \end{bmatrix} \quad (14)$$

assuming the identity matrix as the weight matrix. Different dilution of precision (DOP) parameters can be calculated as follows (Hofmann-Wellenhof 2012):

$$\begin{cases} GDOP = \sqrt{\sigma_{X_r}^2 + \sigma_{Y_r}^2 + \sigma_{Z_r}^2 + \sigma_{cdt}^2} \\ PDOP = \sqrt{\sigma_{X_r}^2 + \sigma_{Y_r}^2 + \sigma_{Z_r}^2} \\ TDOP = \sqrt{\sigma_{cdt}^2} \\ HDOP = \sqrt{\sigma_{E_r}^2 + \sigma_{N_r}^2} \\ VDOP = \sqrt{\sigma_{h_r}^2} \end{cases} \quad (15)$$

where GDOP is geometric dilution of precision, PDOP is position dilution of precision and TDOP is time dilution of precision. HDOP and VDOP are also the dilution of precision in the horizontal position and the vertical component, respectively. It should be noted that $\sigma_{E_r}^2$, $\sigma_{N_r}^2$ and $\sigma_{h_r}^2$ can be computed from transforming the cofactor matrix $Q_{\hat{x}}$ into the LA frame by the law of covariance propagation (Hofmann-Wellenhof 2012). The position of a receiver is assumed to be located in Calgary (51°N, 114°W), AB, Canada with a height of 1115 m. The assumed elevation and azimuth angles are chosen as $E_1 = 30, E_2 = 40, E_3 = 50, E_4 = 60$ degrees and $\alpha_1 = 0, \alpha_2 = 90, \alpha_3 = 180, \alpha_4 = 270$ degrees. In Figure 1, one can also observe the horizontal positioning error distributed in the shape of error ellipses in Case I (without height constraint) and Case II (height constraint UPPP model). In Case I, the ellipse is elongated approximately in the NE direction, whereas in Case II, the error ellipse transforms nearly into a circle, indicating a reduction in the length of the major semi-axes.
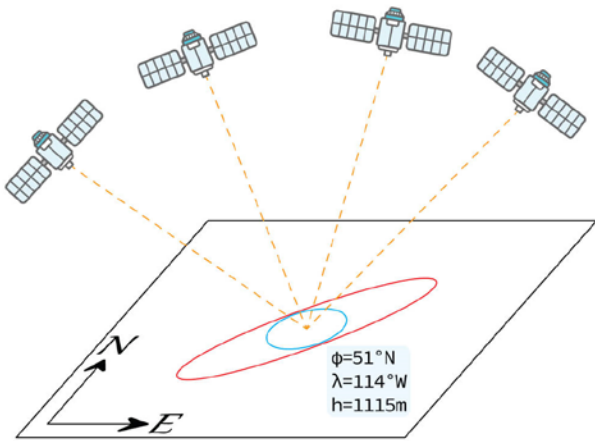

Fig. 1 Simulation setup (red error ellipse: Case I no height constraint and blue error ellipse: Case II height constraint UPPP model)

Figure 2 also illustrates DOP values for Case I (without height constraints) and Case II (height constraint UPPP model). This figure allows us to intuitively observe how the DOP values change when the height constraint is added. The outcomes show that incorporating height constraints not only improves the vertical component estimates but also positively affects the horizontal components estimates as well as the receiver clock error estimate.
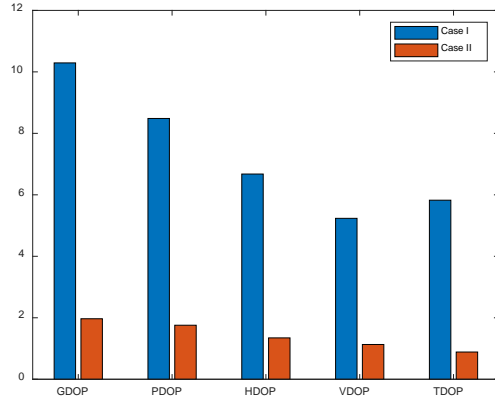

Fig. 2 DOP parameters for Case I and Case II

According to the simulation outcomes, the inclusion of a height constraint is expected to improve the smartphone positioning performance. The next section will further validate this expectation using real datasets, including both walking and on-dash scenarios. "On-dash driving dataset" refers to a dataset collected with a smartphone located on the dashboard of a car while driving.

3. Experimental results

In this section, we will present the positioning results of both pedestrian walking and vehicular on-dash scenarios to evaluate the effect of adding height constraints to PPP model using a dual-frequency Xiaomi Mi8 device. The Xiaomi Mi8, equipped with the Broadcom BCM47755 GNSS chipset, is the world's first dual-frequency GNSS smartphone, i.e., added with L5 for GPS and QZSS and E5a for Galileo (European GNSS Agency, GSA 2018).

3.1 Walking experiment

A walking test was conducted in the parking lot of University of Calgary on 21 April 2021. The test setup and the reference trajectory can be seen in Figure 3. The Xiaomi Mi8 smartphone was placed on the Trimble controller beside the pole. The reference trajectory was obtained from the RTK solution using the commercial post-processed Novatel software called Waypoint. A geodetic receiver setup on a geodetic pillar on the roof of the ENF building (with the true position) was also considered as the base receiver. The vertical level arm between the smartphone and the Trimble R10 antenna was measured and applied while the corresponding horizontal level arm was ignored since it is small enough compared with the positioning accuracy level (around 10 cm). Tables 1 provides GNSS data information and processing setting.
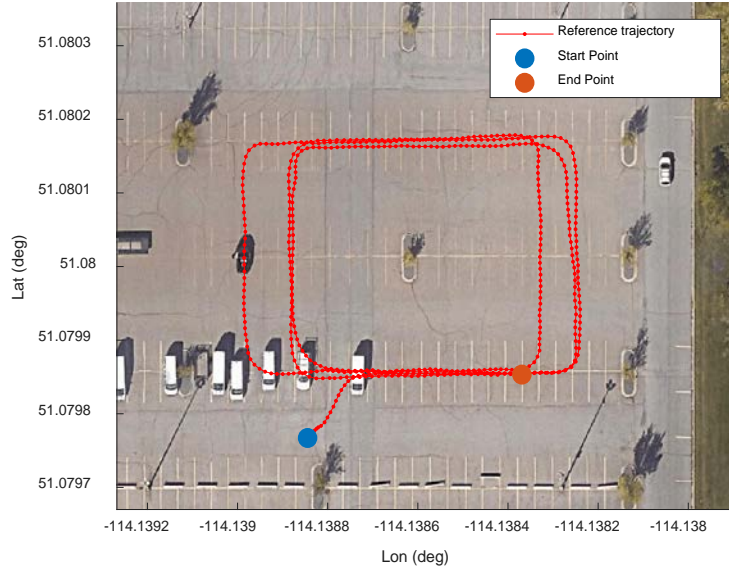
Fig. 3 Walking experiment setup and trajectory (Xiaomi Mi8, April 21, 2021)

Table 1. GNSS data information and processing setting

Device	Xiaomi Mi8
Measurements used	GPS (L1/L5), GLONASS (L1), Galileo (E1/E5a)
Mode	Kinematic
Date	21 April 2021
Duration	10 min
Sampling interval	1 s
Troposphere model	Saastamoinen model (Saastamoinen 1972)
Ionosphere model	Global ionospheric maps (GIM)
Functional model	Case I: UPPP model without height constraint and Case II: height constraint UPPP model
Stochastic model	C/N0 and elevation weighting function (Zangenehnejad and Gao 2023)
Elevation mask angle	10 deg
C/N0 mask	20 dB-Hz
Satellite orbit	CODE MGEX precise ephemerides (5 min interval)
Clock error	CODE MGEX precise clock (1 sec interval)
Satellite DCB correction	CAS DCBs in Bais SINEX (BSX) format

The positioning error is then calculated as the difference between the estimated positions and the true coordinates. First, it is crucial to examine the smartphone vertical error (called receiver solution), as we intend to utilize the smartphone height information as the weighted constraints. Figure 4 provides the receiver vertical error for the walking test on 21 April 2021. As illustrated in the plot, the receiver vertical errors display a smooth behavior with no sudden jumps or anomalies, which is not the case for the PPP solutions employing the GNSS observations. This can be explained by the fact that the chipset solution is not solely reliant on the GNSS observations and incorporates data from other sensors as well. Therefore, it is expected that the receiver's vertical component accuracy is superior to solutions that rely solely on the GNSS data. Consequently, one

may benefit from such better height estimates by considering them as the weighted constraints.
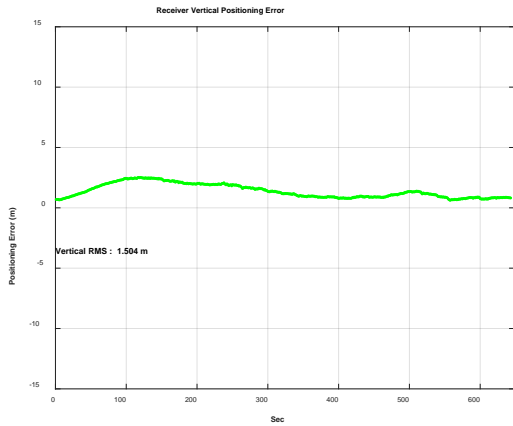

Fig. 4 Receiver vertical error for walking test

Figure 5 also provides the horizontal positioning performance of the UPPP model for the walking test on 21 April 2021 in the two different cases, Case I: UPPP model, Case II: height constraint UPPP model as well as the receiver (smartphone) solution. It also depicts the cumulative distribution error plot of the horizontal positioning error for Case I, Case II and the smartphone solution. Please note that the values displayed in this figure were calculated using all positioning solutions, including the convergence period. A few observations can be highlighted from the figure. (1) Both Case I and Case II solutions outperform the smartphone solution, indicating better performance of our solutions. However, this superiority is not observed during the first 60 seconds
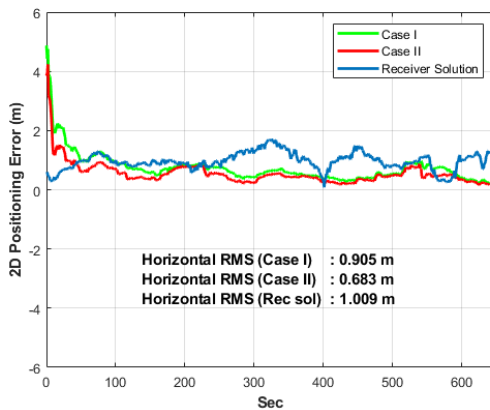
before the PPP convergence occurred. (2) The results indicate that incorporating height constraints into the UPPP model resulted in an improvement in positioning performance, specifically a 24% decrease in horizontal RMS and a 26% decrease in the 50th percentile error. (3) The Case II solution outperforms Case I for the majority of epochs, approximately 99.8% of the entire time.

Tables 2 also provides the East, North and Horizontal RMS values for Case I: UPPP model only, Case II: adding height constraint and the receiver (smartphone) solution. The table also includes the PPP convergence time. It is defined as the time taken to achieve a specific level of positioning accuracy. In this study, convergence is defined as when the horizontal positioning error is less than 1 meter and remains below 1 meter for all subsequent epochs. Using this definition, Case I converged at epoch 97, while Case II achieved convergence at epoch 29, indicating a 70% reduction in convergence time. However, according to this definition, the smartphone solution never achieved convergence. To have a better view, Figure 6 displays the convergence criteria limit (1 m) along with the epochs of convergence depicted by the magenta dashed lines. However, it is important to acknowledge that the convergence statistics might be unreliable based on relatively shorter datasets in this walking dataset. Further analysis of longer datasets therefore would be recommended as a future work.
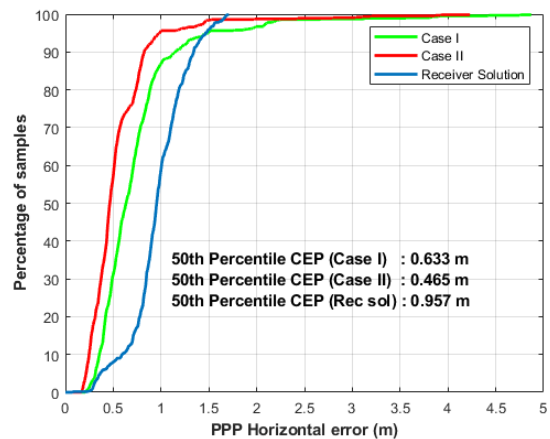

Fig. 5 Horizontal positioning error (left), Cumulative distribution error plot of horizontal positioning error (right) for walking test
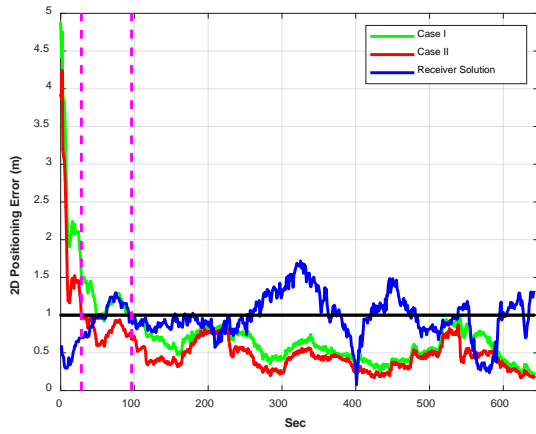
73

Fig. 6 Convergence performance of Case I, Case II and smartphone solution for walking test

3.2 On-dash driving experiment

Two on-dash driving tests were conducted to examine the positioning performance of Case I in comparison to the height constraint UPPP model (Case II). Both datasets were collected on May 10th, 2023, in an open sky environment including overpasses, and in a more challenging environment in
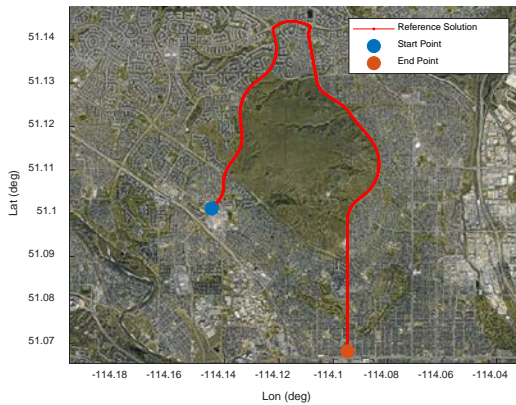
Calgary, Alberta, Canada. The reference trajectories were also obtained from the tightly-coupled RTK/INS solution using the commercial post-processed Novatel software called Waypoint. Similarly, the geodetic receiver located on the roof of the ENF building (was considered as the base receiver. Figure 7 displays the reference vehicle's paths in the two different environments

Table 2 East, North and Horizontal RMS values in meters for Case I: UPPP model only, Case II: height constraint UPPP model and receiver (smartphone) solution

Solutions	East	North	Horizontal	Convergence time (sec)
Case I	0.652	0.627	0.905	97
Case II	0.471	0.494	0.683	29
Rec solution	0.695	0.731	1.009	Not achieved

Fig. 7 On-dash driving trajectories (Left: Open-sky environment, Right: Urban environment)

To validate the smartphone vertical performance, the vertical error plots for both datasets (open-sky and urban environment tests), are presented in Figure 8. In this plot, one can also observe the UPPP only vertical RMS values (Case I with no height constraints). As depicted in the plot, the receiver vertical RMS values are approximately 1.6 and 2.04 meters for the open-sky and urban environments, respectively. Two key points should be highlighted here: (1) They are larger than the corresponding horizontal components RMS values (See Figure 9), which is expected because the GNSS height estimates are typically worse than the horizontal components due to the geometry between the satellites and the

receiver. (2) The UPPP vertical RMS values are larger than those of the smartphone solutions. Morover, the receiver vertical errors display a smooth behavior with no sudden jumps or anomalies, which is not the case for the UPPP only solutions. This can be explained by the fact that the chipset solution is not solely reliant on the GNSS observations and incorporates data from other sensors as well. Therefore, it is expected that the receiver's vertical component accuracy is better than ours, which solely relies on the GNSS data. Consequently, one can benefit from these better height estimates by considering them as the weighted constraints.
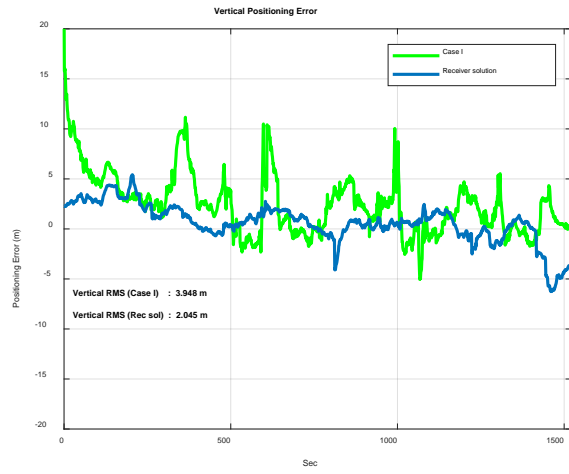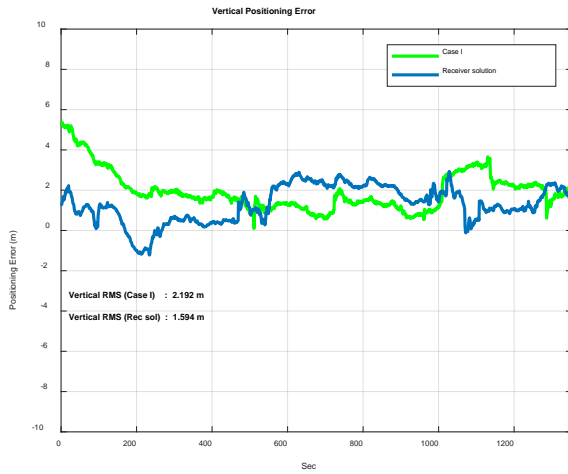
Fig. 8 Vertical positioning error (Left: Open-sky environment test and Right: Urban environment)

Figure 9 provides the horizontal positioning performance of the UPPP model for the on-dash driving test carried out on 10 May 2023 in the open-sky environment in two different cases, Case I: UPPP model only, Case II: height constraint UPPP model. From the figure, a few key points can be highlighted. (1) Adding height constraints into the UPPP model resulted in an improvement in positioning performance with 25% decrease in horizontal RMS and 30% decrease in the 50th percentile error. (2) The maximum error decreased from 1.68 meters to about 1.35 meters when the height constraints added. (3) The Case II solution outperforms Case I for the majority of epochs, approximately 70% of the entire time period. (4) Case I converged at epoch 78, Case II at epoch 32, whereas the smartphone solution did not achieve convergence. It is important to highlight that after about 18 minutes (epoch 1100), the RMS surpassed the selected threshold, remaining increasing for Case I and subsequently decreasing for Case II. Nevertheless, epochs 78 and 32 are still regarded as the convergence epochs.

Finally, we investigate how introducing a height constraint to the UPPP model affects performance in a more challenging environment. The second dataset was collected in Kensington, an urban area in Calgary, on the same date as the open-sky dataset (see Figure 7). Figure 11 illustrates the horizontal positioning performance of the UPPP model for this dataset in two different cases. Tables 3 also provides the East, North, horizontal RMS values and the convergence time for both on-dash datasets. The same conclusion holds true here. (1) Adding height constraints into the UPPP model resulted in an improvement in positioning performance with 18% decrease in horizontal RMS and 22% decrease in the 50th percentile error. (2) The maximum error decreased from approximately 8.51 meters to about 4.73 meters when the height constraints added. (3) The Case II solution outperforms Case I for the majority of epochs, approximately 79% of the entire time period. It is important to note that due to the challenging environment, none of the cases met the convergence criteria.
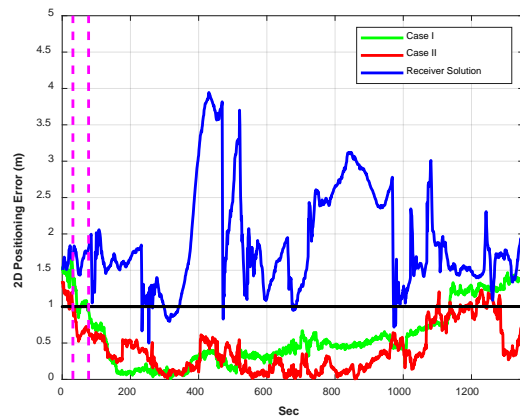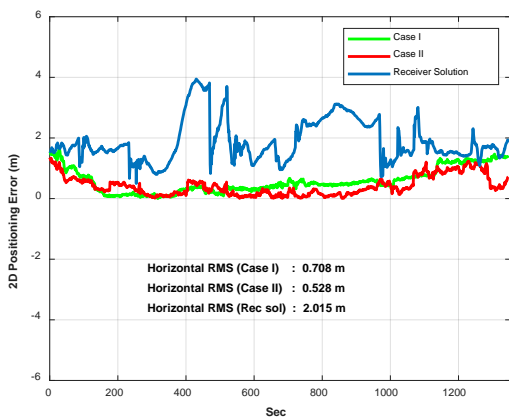

Fig. 9 Horizontal positioning error (left), Cumulative distribution error plot of horizontal positioning error (right) for open-sky driving test

Fig. 10 Convergence performance of Case I, Case II and smartphone solution for open sky driving test
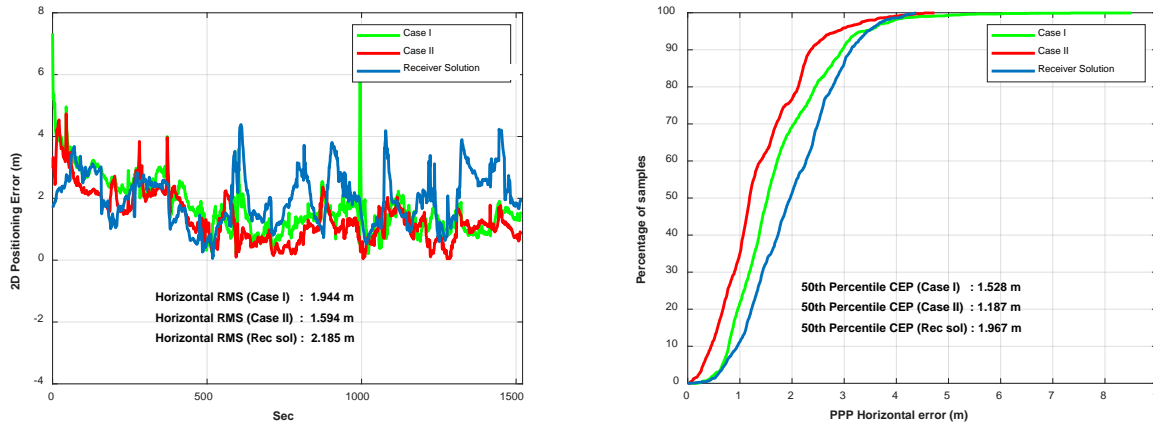
Fig. 11 Horizontal positioning error (left), Cumulative distribution error plot of horizontal positioning error (right) for urban area driving test

4. Summary and conclusions

Since Android version 7's release in 2016, smartphone users gained access to the raw GNSS measurements via the android.location API (API level 24). Since then, the utilization of smartphones for various applications such as cadastral surveying, mapping surveying applications, and navigation has been significantly increasing due to the cost-effective GNSS smartphones. Despite a focus on using the smartphone GNSS observations in many studies, this research considered the impact of incorporating the height information on the smartphone-based positioning. It is expected that the incorporation of height information significantly improves the overall solution, even with the inherent lower vertical accuracy of GNSS. This is because it increases the degree of freedom and strengthens the geometry of the receiver and satellites. This study specifically evaluated the uncombined PPP model performance while the height constraints were introduced to the model. Several datasets from both pedestrian walking and vehicular scenarios with a dual-frequency Xiaomi Mi8 device were utilized. The results demonstrate notable enhancements. The conclusions of our study are listed as follows:

1- In the walking test, the results showed an improvement of 24% and 26% on the RMS of horizontal error and the 50th percentile error, respectively, when employing the height constraints UPPP model (Case II). Additionally, Case II demonstrated a remarkable 70% reduction in the PPP convergence time.

2- In the open-sky environment scenario, the results confirmed a 25% decrease in the horizontal RMS and a 30% decrease in the 50th percentile error, when employing the height constraints UPPP model (Case II). Similar to the walking test, this dataset also revealed a decrease in PPP

convergence time, providing further support for the positive impact of incorporating height constraints.

Table 3 East, North and Horizontal RMS values in meters for Case I: UPPP model only, Case II: height constraint UPPP model and receiver (smartphone) solution for kinematic experiment

Dataset	Solution	East	North	Horizontal	Convergence time (sec)
Dataset 1	Case I	0.580	0.406	0.708	78
	Case II	0.378	0.368	0.528	32
	Rec solution	1.543	1.295	2.015	Not achieved
Dataset 2	Case I	1.101	1.623	1.944	Not achieved
	Case II	1.166	1.087	1.594	Not achieved
	Rec solution	1.593	1.496	2.185	Not achieved

3- In the more challenging environment scenario, utilizing the height constraints (Case II) resulted in an 18% reduction in horizontal RMS and a 22% decrease in the 50th percentile error. Additionally, the maximum error decreased from approximately 8.51 meters to about 4.73 meters when the height constraint was added. However, due to the challenging environment, none of the cases met the convergence criteria.

In our future research, we plan to employ the smartphone's barometer to estimate height using the atmospheric pressure. It can be helpful particularly in downtown areas where the GNSS signals may face blockage mainly caused by the presence of tall buildings in those areas.

References

Abdulrahim, K., Hide, C., Moore, T., Hill, C. (2012) Using constraints for shoe mounted indoor pedestrian navigation. *Journal of Navigation*, 65(1), 15-28.

Albéri M., Baldoncini M., Bottardi C., Chiarelli E., Fiorentini G., Kgc R., Realini E., Reguzzoni M., Rossi L. (2017), Sampietro D. Accuracy of flight altitude measured with low-cost GNSS, radar and barometer sensors: Implications for airborne radiometric surveys, *Sensors*, 17(8), 1889.

Chen, B., Gao, C., Liu, Y., and Sun, P. (2019), Real-time precise point positioning with a Xiaomi MI 8 android smartphone. *Sensors*, 19(12), 2835.

Elmezayen, A., and El-Rabbany, A. (2019). Precise point positioning using world's first dual-frequency GPS/GALILEO smartphone. *Sensors*, 19(11), 2593.

European Global Navigation Satellite Systems Agency, GSA (2018), Worlds first dual-frequency GNSS smartphone hits the market GSA. Available at: https://www.gsa.europa.eu/newsroom/news/world-s-first-dual-frequency-gnss-smartphone-hits-market [Accessed 24 November 2023].

Guo, L., Wang, F., Sang, J., Lin, X., Gong, X., Zhang, W. (2020). Characteristics analysis of raw multi-GNSS measurement from Xiaomi Mi 8 and positioning performance improvement with L5/E5 frequency in an urban environment. *Remote Sensing*, 12(4), 744.

Héroux, P., Gao, Y., Kouba, J., Lahaye, F., Mireault, Y., Collins, P., Macleod, K., Tetreault, P., Chen, K. (2004), Products and applications for precise point positioning - moving towards real-time, *In Proceedings of the 17th international technical meeting of the satellite division of The Institute of Navigation (ION GNSS 2004)* Long Beach, CA, 2004., (pp. 1832-1843).

Hofmann-Wellenhof, B., Lichtenegger, H., and Collins, J. (2012), *Global positioning system: theory and practice*, Springer Science & Business Media.

Kim, Y., Hwang, Y., Choi, S., Lee, J. (2013), Height estimation scheme of low-cost pedestrian dead-reckoning system using Kalman filter and walk condition estimation algorithm. *In 2013 IEEE/ASME International Conference on Advanced Intelligent Mechatronics* (pp. 1492-1497). IEEE.

Kouba, J., and Héroux, P. (2001), Precise point positioning using IGS orbit and clock products, *GPS Solution*, 5(2), 12-28.

Landa, V., Ben-Moshe, B., Hacohen, S., and Shvalb, N. (2018), GoIn-An Accurate 3D InDoor Navigation Framework for Mobile Devices. *In 2018 International Conference on Indoor Positioning and Indoor Navigation (IPIN),* (pp. 1-8). IEEE.

Li, Y., and Cai, C. (2022), A Mixed Single-and Dual-Frequency Quad-Constellation GNSS Precise Point Positioning Approach on Xiaomi Mi8 Smartphones, *The Journal of Navigation,* 75(4), 849–863.

Li, Y., Cai, C., and Xu, Z.A. (2022a), Combined Elevation Angle and C/N0 Weighting Method for GNSS PPP on Xiaomi MI8 Smartphones, *Sensors*, 22(7), 2804.

Li, X., Wang, H., Li, X., Li, L., Lv, H., Shen, Z., Xia, C., Gou, H. (2022b), PPP Rapid Ambiguity Resolution using Android GNSS Raw Measurements with a Low-Cost Helical Antenna, *Journal of Geodesy*, 96(10), 65.

Li, M., Huang, T., Li, W., Zhao, Q., and Jiang, K. (2023), Precise point positioning with mixed single-and dual-frequency GNSS observations from Android smartphones considering code-carrier inconsistency. *Advances in Space Research*.

Liu, R., Guo, B., Zhang, A., and Yimwadsana, B. (2020), Research on GPS precise point positioning algorithm with a Sea Surface Height Constraint, *Ocean Engineering*, 197, 106826.

Montenbruck, O., Hauschild, A., and Steigenberger, P. (2014), Differential code bias estimation using multi-GNSS observations and global ionosphere maps, *Navigation*, 61, 191–201.

Phatak, M., Chansarkar, M., and Kohli, S. (1999), Position fix from three GPS satellites and altitude: a direct method, *IEEE Transactions on Aerospace and Electronic Systems*, 35(1), 350-354.

Paziewski, J. (2020), Recent Advances and perspectives for positioning and applications with smartphone GNSS observations. *Measurement Science and Technology,* 31(9), 091001.

Saastamoinen, J. (1972), Atmospheric correction for the troposphere and stratosphere in radio ranging satellites. *The use of artificial satellites for geodesy*,15, 247–251.

Shin, B., Kim, C., Kim, J., Lee, S., Kee, C., Kim, H. S., and Lee, T. (2016), Motion recognition-based 3D pedestrian navigation system using smartphone, *IEEE Sensors Journal*, 16(18), 6977-6989.

Teunissen, P.J.G., and Kleusberg, A. (1998), *GPS for Geodesy (2nd ed.),* Berlin-Heidelberg-New York: Springer-Verlag.

Wang, N., Yuan, Y., Li, Z., and Tan, B. (2016), Determination of differential code biases with multi-GNSS observations, *Journal of Geodesy*, 90, 209–28

Wu, Q., Sun, M., Zhou, C. and Zhang, P. (2019). Precise point positioning using dual-frequency GNSS observations on smartphone, *Sensors*, 19(9), 2189.

Yi, D., Yang, S., and Bisnath, S. (2022), Native smartphone single-and dual-frequency GNSS-PPP/IMU solution in real-world driving scenarios, *Remote Sensing*, 14(14), 3286.

Zangenehnejad, F., and Gao, Y. (2021), GNSS Smartphones Positioning: Advances, Challenges, Opportunities, and Future Perspectives, *Satellite Navigation*, 2, 24.

Zangenehnejad, F., and Gao, Y. (2023), Stochastic modeling of smartphones GNSS observations using LS-VCE and application to Samsung S20, *Sensors*, 23(7), 3478.

Zhao, H., Cheng, W., Yang, N., Qiu, S., Wang, Z., and Wang, J. (2019), Smartphone-based 3D indoor pedestrian positioning through multi-modal data fusion, *Sensors*, 19(20), 4554.

Zhu, H., Xia, L., Li, Q., Xia, J., Cai, Y. (2022), IMU-Aided Precise Point Positioning Performance Assessment with Smartphones in GNSS-Degraded Urban Environments, *Remote Sensing*, 14(18), 4469.

Zumberge, J.F., Heflin, M.B., Jefferson, D.C., Watkins, M.M., and Webb, F. H. (1997), Precise point positioning for the efficient and robust analysis of GPS data from large networks, *Journal of geophysical research: solid earth*, 102(B3), 5005-5017.

Authors

Farzaneh Zangenehnejad is a PhD student under the supervision of Dr. Yang Gao in the Department of Geomatics Engineering at the University of Calgary, Canada. Her research focuses on GNSS-based positioning, GNSS processing techniques, and low-cost and smartphone positioning.

Dr. Yang Gao is a Professor in the Department of Geomatics Engineering at the University of Calgary, Canada. His research expertise includes both theoretical aspects and practical applications of satellite-based precise positioning systems and multi-sensor integrated systems. His academic and leadership contributions have been recognized by national and international awards and he is a Fellow of the US Institute of Navigation (ION), the International Association of Geodesy (IAG), the Engineering Institute of Canada (EIC) and the UK Royal Institute of Navigation (RIN).